5-2024

Better Light than Never: A New Radiative Mechanism for Observing Binary Black Holes

Paul Rioles
University of Massachusetts Boston

BETTER LIGHT THAN NEVER:
A NEW RADIATIVE MECHANISM FOR OBSERVING BINARY BLACK HOLES

A Thesis Presented

by

PAUL RIOLES

Submitted to the Office of Graduate Studies, University of Massachusetts Boston, in partial fulfillment of the requirements for the degree of

MASTER OF SCIENCE

May 2024

Applied Physics Program

BETTER LIGHT THAN NEVER:

A NEW RADIATIVE MECHANISM FOR OBSERVING BINARY BLACK HOLES

A Thesis Presented

by

PAUL RIOLES

Approved as to style and content by:

Chandra Yelleswarapu , Associate Professor
Chairperson of Committee

Stephen Arnason , Associate Professor
Member

Jonathan Celli , Professor
Member

Jonathan Celli, Program Director
Applied Physics Program

Rahul Kulkarni, Chairperson
Physics Department

ABSTRACT

BETTER LIGHT THAN NEVER:
A NEW RADIATIVE MECHANISM FOR OBSERVING BINARY BLACK HOLES

May 2024

Paul Rioles,
B.A., Clark University
M.S., University of Massachusetts Boston

Directed by Associate Professor Chandra Yelleswarapu

Black holes are notoriously elusive, they are impossible to observe directly, and current methods of extracting information from behind their cosmic camouflage are both limited in number and experimentally difficult. The scope of this investigation is to explore a proposed novel radiative mechanism for active similar mass binary black holes, affording new observational methods to investigate frequency inspirals of BH mergers. The explored mechanism is a result of each BH's accretion of the surrounding plasma, creating voids that orbit throughout the plasma. The significant results described in this thesis include expressions for the frequency, power radiated per unit solid angle, and average power radiated for the quadrupolar radiation of our system.

TABLE OF CONTENTS

CHAPTER Page

LIST OF FIGURES

Figure Page

CHAPTER 1

INTRODUCTION

1.1 Black Hole Observation

Black Holes have stood brazenly at the pinnacle of scientific curiosity dating back to their inception when Karl Schwarzschild first presented his solution to Einstein's field equations of general relativity in 1916 [1]. These aforementioned cosmic beasts test the limits of even our most proven theories, and deciphering the underlying physics that governs them is justifiably the pièce de résistance to which many researchers aspire. Unfortunately for us, black holes are intrinsically uncooperative. Their extreme curvature of space-time requires that anything that crosses the black hole's event horizon is henceforth inaccessible to the rest of the universe. The short of it: Light and matter being irrecoverable after a direct encounter with a black hole does not bode well for the measurability of its characteristics and behaviors.

Nevertheless, efforts trudged onwards. One of the first major observations in the field was born from the investigation of a galactic X-ray source dubbed Cygnus X-1. The teams of astronomers involved established that the X-ray source was not associated with any of the bright objects in the region, but rather some unusual object whose brightness fell below the resolvable range of their equipment [2]. In the following years, after significant squabble, the astronomical community came to the consensus that the 1971 observations had in fact discovered the first black hole [3]. A necessary distinction must be drawn here: The black hole was not directly emitting the X-rays, but rather the black hole was pulling on the gas from a nearby star, accelerating and therefore heating it

tremendously at which point the transiting gas was emitting X-rays. The significance being, observation was limited to indirect evidence based on the above statement that nothing can escape the event horizon of a black hole.

That was until Stephen Hawking, in hero-esque fashion, further revolutionized the field with his theoretical formulation of Hawking Radiation in 1974 [4]. He showed that black holes, being ideal black bodies, should thermally radiate and as a result, eventually evaporate. The first example of emission directly from a black hole! Unfortunately, Hawking radiation fails to directly add to the observationalist's toolbox as the incredibly low temperatures of reasonably sized black holes imply an irrecoverably small power radiated [5].

With direct emission not panning out in an observational sense, researchers are forced into creativity in their quest to shed light on our universes darkest objects. Take the Event Horizon Telescope project for example. A global array of telescopes unified seamlessly via very long baseline interferometry in order to create a virtual reflector the size of planet Earth [6]. A necessary undertaking, as the wavelengths associated with radio astronomy demand larger reflectors for fractions of the resolutions achievable through other forms of observational astronomy. EHT's ingenuity paid off when their array finally generated the first image of a black hole, utilizing the radio emissions of the accelerated gas in the accretion disk which surrounds the black hole. Fig. 1 [7].

The nature of this EHT observation categorically demonstrates the nature of thinking intended to be conveyed throughout this thesis. Black holes themselves are shrouded in a defensive boundary of darkness, meaning our best observational tools are those systems directly, but externally, correlated to the characteristics of black holes. I intend to explore and share a novel radiative mechanism apparent in active binary black holes, offering a new tool in astronomers limited arsenal to study the behaviors of these astronomical oddities.

Figure 1: Radio image of the supermassive black hole at the center of the Messier 87 galaxy captured by the EHT team, showcasing the utility of observing closely coupled systems external to the black hole rather than the hidden black hole itself.

1.2 Intended Contribution

The mechanism of interest, as I will derive, is a result of the time-dependent electric quadrupole moment associated with the plasma dynamics of the accretion disk surrounding binary black holes. While computationally such a problem sounds rather unpleasant, I assert that the components of interest emerge with little effort. The complexities manifest themselves in the formulation of radiative power, an important measure, but one whose exact determination is of lesser significance in this investigation.

CHAPTER 2

SYSTEM IN CONSIDERATION

In order to produce the previously mentioned quadrupole radiation, the system must necessarily be a binary pair of ”active” similar mass black holes. Where active refers to the BH's active accretion of (absorbing and as a result gaining mass from) the surrounding matter in an accretion disk. Justifying these necessary conditions calls for a more detailed depiction of the system, so allow me to supplement our imagination with some simplified diagrams.

2.1 Binary Black Hole System

Firstly, we are looking initially to describe our novel radiation through a simple model which can later be more thoughtfully expanded upon. In the interest of simplicity, we enforce the above condition that our binary system be composed of two equal mass black holes, $M_{BH1} = M_{BH2} = M$, which allows us to model the orbit of each black hole as ideal circular motion with a uniform orbital radius denoted a. Additionally, it will be beneficial for our coming discussion to introduce the idea of the innermost stable circular orbit. ISCO's are the last stable circular orbits, nearest to the black hole, past which any circularly orbiting matter will succumb to the extreme gravitational potentials associated with the black hole and plunge to their eternal imprisonment [8]. The described binary system depicting two BH's circularly orbiting each other with some frequency, and an external ISCO can be seen in Fig. 2

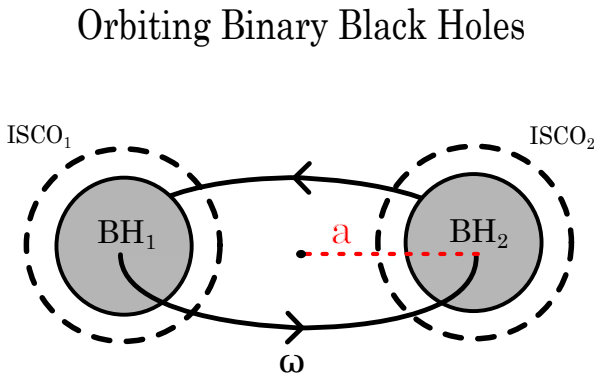

Figure 2: Illustration of same mass binary black hole orbits. Here a is the orbital radius, ISCO corresponds to the innermost stable circular orbit of each black hole, and ω represents the orbital frequency

2.2 Binary System in an Accretion Disk

With the image of a binary black hole system (as we have simply described it) freshly in our minds, let us now further expand our system by placing the BH's in a dense plasma. This environment is not new to our BH's. Being the densest and most massive celestial bodies in the universe, these objects have a habit of collecting other matter. Particularly, black holes are often surrounded by large collections of gas. As the infalling matter concentrates towards the massive body, it typically has an associated angular momentum which leads to the formation of an infalling disk of matter [9]. As the matter is accelerated toward the black hole, the interactions between fast-moving particles increases the matter's thermal energy. Eventually, overcoming the electron binding energy, resulting in the formation of a plasma. That being said, let us now envision our binary black holes surrounded by the plasma of an accretion disk. Such a system is presented in the illus-

tration in Fig. 3. Figure 3 offers a zoomed in frame of the binary black holes surrounded

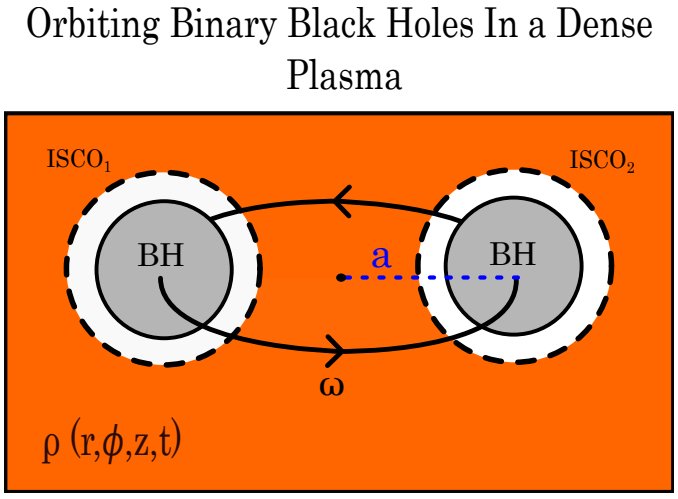

Figure 3: Illustration of our binary system surrounded by the plasma of an accompanying accretion disk. The charge density of such a plasma will generally have a radial, angular, height, and time dependence throughout the disk.

by the plasma inside an accretion disk. In reality the disk typically extends well beyond the characteristic scale of our binary system. Often accretion disks are measured in light-days [10] a unit which dwarfs typical orbital radii of the BH's, especially towards the binary inspiral and merger.

2.3 Plasma Holes

It is important to take note here, the innermost stable circular orbit of the black holes act as absorbing spheres in this plasma. The surrounding matter is accreted, removing it from the accretion disk. As the binary BH's co-rotate through the accretion disk, they attempt to carve out the volume of a swept torus where the voids they create are quickly filled in by the surrounding plasma rushing to disperse its charge through this newly

formed void [11]. In this investigation, we are interested not in the black holes themselves, but rather we will leverage these so-called plasma voids that rotate around each other, mirroring the motion of the two black holes. A simple illustration of the rotating plasma holes (the true heroes of our story) is shown in Fig. 4 In order to derive the

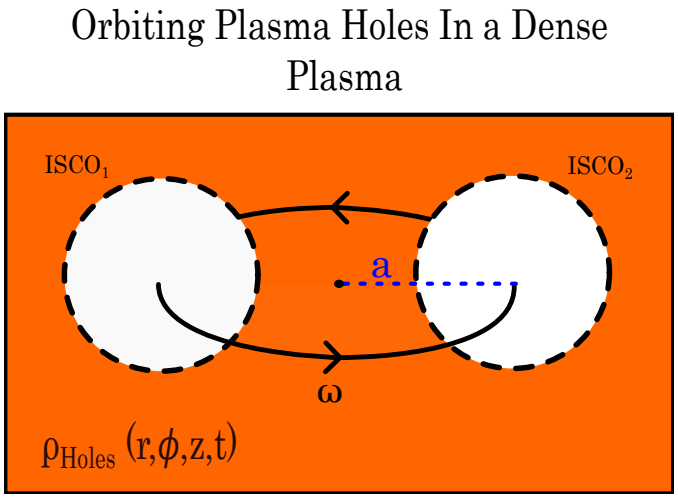

Figure 4: Depiction of the co-rotating plasma voids left by the binary black holes' accretion of matter throughout their orbital cycles.

significance of this plasma distribution, we will utilize the principle of linear superposition for electric charges. This is perhaps the highest friction point within this entire model. At incredibly high electric field strengths (whose exact value is determined by the Schwinger Limit) nonlinear electromagnetic effects become prominent [12]. In this case, adding or decomposing nonlinear quantities becomes much more complex [13]. Seeing as though this is the initial exploration of a new astrophysical mechanism whose characteristic electric field magnitudes are not yet known, allow me to first derive our model considering classical, linear electrodynamics: From which, depending on the resolved orders of magnitude within our results, we can determine whether more careful evaluation is necessary. Additionally, there is a massive range in disk size and den-

sity of matter in accretion disks throughout the universe. Considering that the disk's matter density would significantly effect the accretion rate of any encompassed black holes, there must certainly be some sizable range of lower plasma density accretion disks where the suggested linear superposition of charge indeed holds.

That being said, assuming linearity for now, we can approach the hole in our charge density shown in Fig. 4 as a decomposition of the charge distribution in the accretion disk without any holes minus our two absorbed spheres of charge. This is easier understood pictorially, so turn your attention to Fig. 5 where we demonstrate the application of superposition in this scenario.

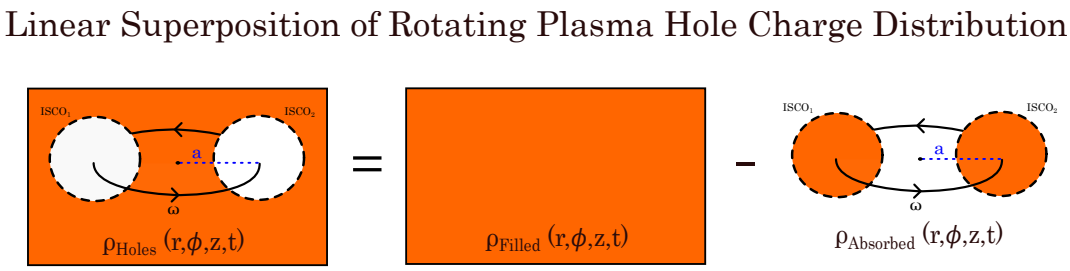

Figure 5: Decomposition of the orbiting plasma hole charge distribution into its two components: the complete charge distribution of the accretion disk and the spheres of charge being removed by each black hole every cycle.

Now, we are armed with the necessary weaponry to explore the potential radiative mechanism hiding within our original charge distribution. As shown in an example by Professor Steve Arnason [14], charges that are equally spaced out and rotating around the circumference of a circle have time dependent multipole moments (a much more in depth discussion and derivation of the multipole expansion is coming in the next chapter) which radiate. However, as you continue adding charges, the magnitude of radiated power falls dramatically, and in the limit of infinite charges around your circle, you

find that time-dependence falls out of the resulting charged ring, and therefore there is no longer any radiation emitted from that system. Point being, on small scales the plasma inside the accretion disk can have chaotic behavior, but on large scales the disk is relatively uniform [15]. This implies, even if there is a time dependent non-vanishing electric multipole term, the radiated power should be significantly reduced compared to lower order terms. This reduction is due to a high uniformity over time, a mechanism similar to what was derived in the previously mentioned circle of rotating charges example provided by Prof. Arnason. This implies that the first terms in our superposition decomposition need not be considered in regards to electric multipole radiation. However, we should take more care when considering the second term in the superposition. We have two spheres of like charge, whose signs are opposite that of the physical charge absorbed by each black hole. These spheres of charge co-rotate around one another with the orbital radius and frequency of the binary black holes. It can (and will in the next chapter) be shown that this charge distribution will in fact have an associated time dependent multipole moment, and therefore produce multipole radiation.

2.4 Point Charge Model

Continuing the construction of our simple model, we can approximate these co-rotating spheres of charge with points of charge rotating around a circle, where each point charge is equal to the enclosed charge within our spheres. We will express the characteristics of this mathematical model and work through the process of calculating radiation from such a model in chapter 3.

CHAPTER 3

ELECTRIC MULTIPOLE RADIATION

The electric multipole expansion is a series expansion of the electric potential into terms with increasingly complex angular structure and inverse powers of radial distance to the origin. In totality, the multipole expansion is an exact representation of the original electric potential, however the lowest order surviving term dominates the expansion, proving to approximate the original system well.

For our described system of interest, the symmetries of the rotating charges induce an electric potential which are dominated by the electric quadrupole moment.

The following calculations and their application were inspired by a similar exercise presented by Professor Steve Arnason in our Classical Electricity and Magnetism course. Various equations and strategies were derived from his class notes and problem set solutions, the former of which I have included in my references here [14]. Carrying on.

3.1 Deriving the Charge Density of the Rotating Point Charge System

Modeling the previously discussed rotating plasma spheres as rotating point charges, we will employ the help of Dirac delta functions to formulate our charge distribution.

$$\rho(\vec{r},t) = \sum_{n=1}^{2} q_n \delta(\vec{r} - \vec{r_n}') \tag{3.1}$$

Where $\vec{r_j}'$ is constructed as

$$\vec{r_n}' = \sum_{n=1}^{2} (\vec{x}_n + \vec{y}_n) \tag{3.2}$$

$$\vec{x}_n' = a\cos(\pi n - \omega t)\hat{x} \tag{3.3}$$

$$\vec{y}_n' = a\sin(\pi n - \omega t)\hat{y} \tag{3.4}$$

Where a refers to the orbital radius of the plasma spheres. All together, this expression of our charges' positions yeild the charge density

$$\rho(\vec{r},t) = \sum_{j=1}^{2} q_j \delta\left(\vec{r} - a\cos[\pi n - \omega t]\hat{x} + a\sin[\pi n - \omega t]\hat{y}\right). \tag{3.5}$$

3.2 Vanishing Electric Dipole Moment

To demonstrate the system's vanishing dipole moment, we turn to the expression for a dipole moment considering a system of point charges.

$$\vec{p} \;=\; \sum_{n=2}^{2} q_n \vec{r}_n \tag{3.6}$$

Which for our distribution yeilds,

$$\vec{p} \;=\; q_1\vec{r}_1 + q_2\vec{r}_2. \tag{3.7}$$

At this point, we must recall the previously mentioned condition that we are dealing with black holes of the same mass, and therefore the plasma surrounding the black holes is distributed symmetrically via a symmetric gravitational potential from both objects. This condition allows us to claim that each black hole lies within a mirrored plasma distribution, and therefore should be absorbing equal amounts of charge. So, setting $q_1 = q_2 = q$,

$$\vec{p} \;=\; q\vec{r}_1 + q\vec{r}_2 \tag{3.8}$$

$$\vec{p} \;=\; q\,[\vec{r}_1 + \vec{r}_2] \tag{3.9}$$

Seeing as though the radius for each charge has the same magnitude and opposite direction, we see

$$\vec{p} \;=\; q\,[a\hat{a} - a\hat{a}] = 0 \tag{3.10}$$

We witness the vanishing dipole moment of our system. Implying the electric quadrupole moment will dominate this system's potential.

3.3 Deriving the Electric Quadrupole Moment Tensor

Evaluating the electric quadruple moment requires a more rigorous mathematical adventure which begins, as any great story, with tears. The Quadrupole moment tensor is a 3x3 symmetric traceless matrix described by the equation below, whose enties are related to the five spherical harmonics associated with $\ell = 2$ [14].

$$Q_{ij} = \int d^3\vec{r}\,(3r'_i r'_j - r'^2\delta_{ij})\rho(\vec{r}) \tag{3.11}$$

The tensor must be evaluated entry by entry, lets start with Q_{zz}.

$$Q_{zz} = \int d^3\vec{r}\,(3z'^2_n - r'^2_n)\rho(\vec{r},t) \tag{3.12}$$

Here, seeing as though the motion in our model is confined to two dimensions in the XY-plane, $z' = 0$ and our integral is reduced to two dimensions. Additionally,
$r'^2 = x'^2 + y'^2$.

$$Q_{zz} = \int d^2\vec{r}\,(-(x'^2_n + y'^2_n))\rho(\vec{r},t) \tag{3.13}$$

Substituting in our expressions we get

$$Q_{zz} = -\int d^2\vec{r}\,\sum_{n=1}^{2}(a^2\cos^2(\pi n - \omega t) + a^2\sin^2(\pi n - \omega t))q_n\delta(\vec{r} - \vec{r}_n{}'). \tag{3.14}$$

Using the Pythagorean identity $\sin^2\theta + \cos^2\theta = 1$, we can reduce the expression to

$$Q_{zz} = -a^2\sum_{n=1}^{2} q_n \int d^2\vec{r}\;\delta(\vec{r} - \vec{r}_n{}'). \tag{3.15}$$

Where we know the integral over the Dirac delta function in our charge density is equal to one, and evaluating the sum over our charges yields

$$Q_{zz} = -a^2(q_1 + q_2) = -2qa^2. \tag{3.16}$$

Once again evoking the fact that our two black holes are of the same mass, and therefore we assume the plasma distribution among the binary pair is mirrored for each BH giving our superimposed plasma spheres the same absorbed charge.

Moving onto our next matrix element, lets solve for Q_{yy}

$$Q_{yy} = \int d^2\vec{r}\,(3y_n'^2 - r_n'^2)\rho(\vec{r},t) \tag{3.17}$$

Substituting in our expression for y' along with reusing the fact that r'^2 evaluates to a^2 (from Eq. 3.14) we find

$$Q_{yy} = \int d^2\vec{r} \sum_{n=1}^{2} (3a^2\sin^2(\pi n - \omega t) - a^2) q_n \delta(\vec{r} - \vec{r}_n{}'). \tag{3.18}$$

Pulling everything that is not a function of our variables of integration out in front

$$Q_{yy} = a^2 \sum_{n=1}^{2} q_n \left[3\sin^2(\pi n - \omega t) - 1\right] \int d^3\vec{r}\,\delta(\vec{r} - \vec{r}_n{}') \tag{3.19}$$

Integrating over our delta function once again evaluates to one.

$$Q_{yy} = a^2 \sum_{n=1}^{2} q_n \left[3\sin^2(\pi n - \omega t) - 1\right] \tag{3.20}$$

Now with a barrage of double-angle trig identities, the expression becomes

$$Q_{yy} = a^2 \sum_{n=1}^{2} q_n \left[3\left(\frac{2}{2}[\cos^2(\pi n - \omega t) - \cos(2\pi n - 2\omega t)]\right) - 1\right]. \tag{3.21}$$

$$Q_{yy} = a^2 \sum_{n=1}^{2} q_n \left[\left(\frac{3}{2}[\cos(2\pi n - 2\omega t) + 1 - 2\cos(2\pi n - 2\omega t)\right) - 1\right] \tag{3.22}$$

$$Q_{yy} = a^2 \sum_{n=1}^{2} q_n \left[\left(\frac{3}{2}[1 - \cos(2\pi n - 2\omega t)\right) - 1\right] \tag{3.23}$$

$$Q_{yy} = a^2 \sum_{n=1}^{2} q_n \left[\frac{1}{2} - \frac{3}{2}\cos(2\pi n - 2\omega t)\right] \tag{3.24}$$

Expanding using the difference formula for cosine (Ptolemy's identity), we find

$$Q_{yy} = a^2 \sum_{n=1}^{2} q_n \left[\frac{1}{2} - \frac{3}{2}[\cos(2\pi n)\cos(2\omega t) + \sin(2\pi n)\sin(2\omega t)]\right]. \tag{3.25}$$

Carrying out the summation we get an amalgamation of two of these expanded trig products, in the interest of clarity I will write them separately.

$$n = 1: \quad \cos(2\pi)\cos(2\omega t) + \sin(2\pi)\sin(2\omega t) \tag{3.26}$$

$$n = 2: \quad \cos(4\pi)\cos(2\omega t) + \sin(4\pi)\sin(2\omega t) \tag{3.27}$$

Noting that both $\cos(2\pi) = \cos(4\pi) = 1$, and $\sin(2\pi) = \sin(4\pi) = 0$, our amalgamation simplifies greatly.

$$Q_{yy} = qa^2 \left[\frac{1}{2} - \frac{3}{2}\cos(2\omega t) + \frac{1}{2} - \frac{3}{2}\cos(2\omega t)\right] \tag{3.28}$$

$$Q_{yy} = qa^2 [1 - 3\cos(2\omega t)] \tag{3.29}$$

Giving us our first time-dependent and therefore radiative term.

Moving on to our last diagonal entry Q_{xx}, we can use the nifty property that the trace of our matrix equals zero to determine the last term rather than calculating it out manually. Although, it can be done in much similarity to Q_{yy}.

$$Q_{xx} + Q_{yy} + Q_{zz} = 0 \tag{3.30}$$

$$Q_{xx} = -Q_{yy} - Q_{zz} \tag{3.31}$$

$$Q_{xx} = -qa^2 [1 - 3\cos(2\omega t)] - (-2qa^2) \tag{3.32}$$

$$Q_{xx} = qa^2 [1 + 3\cos(2\omega t)] \tag{3.33}$$

Voila! Now, we must turn to the off-diagonal terms. Luckily, many of them simplify! As we saw in the above derivation of Q_{zz} (3.12), our system's confinement to the x and y

dimensions imply that if either of the $r'_i r'_j$ or $r'^2\delta_{ij}$ terms from equation 3.11 depend on z' they will be sent to zero. Keeping spirits high, this consequently sends any off-diagonal term with z' dependence to zero.

$$Q_{zx} = Q_{zy} = Q_{xz} = Q_{yz} = 0 \tag{3.34}$$

This leaves us with Q_{xy} and Q_{yx}. Once again we find ourselves in quite a fortunate position. Due to the symmetry of the quadrupole moment matrix, $Q_{xy} = Q_{yx}$, so if we determine one we know the other. Starting off, the delta function is not satisfied for off-diagonal entries, so we are only left with the $r'_i r'_j$ term.

$$Q_{xy} = \int d^2\vec{r}\,(3x'_n y'_n)\rho(\vec{r},t) \tag{3.35}$$

$$Q_{xy} = \int d^2\vec{r}\,\sum_{n=1}^{2} 3a\cos(\pi n - \omega t)a\sin(\pi n - \omega t)q_n\delta(\vec{r} - \vec{r_n}') \tag{3.36}$$

Integrating over our delta function and using a trigonometric product identity for sine and cosine, the expression simplifies to

$$Q_{xy} = \sum_{n=1}^{2}\frac{3}{2}q_n a^2[\sin(\pi n - \omega t + \pi n - \omega t) + \sin(\pi n - \omega t - \pi n + \omega t)] \tag{3.37}$$

$$Q_{xy} = \sum_{n=1}^{2}\frac{3}{2}q_n a^2[\sin(2\pi n - 2\omega t) + \sin(0)] \tag{3.38}$$

Applying the sine difference formula,

$$Q_{xy} = \sum_{n=1}^{2}\frac{3}{2}q_n a^2[\sin(2\pi n)\cos(2\omega t) - \cos(2\pi n)\sin(2\omega t)] \tag{3.39}$$

Expanding the sum and once again breaking the equation down for clarity,

$$n = 1: \quad \sin(2\pi)\cos(2\omega t) - \cos(2\pi)\sin(2\omega t) \tag{3.40}$$

$$n = 2: \quad \sin(4\pi)\cos(2\omega t) - \cos(4\pi)\sin(2\omega t) \tag{3.41}$$

Recalling that $\sin(2\pi) = \sin(4\pi) = 0$ and $\cos(2\pi) = \cos(4\pi) = 1$, the expression simplifies to

$$Q_{xy} = \frac{3}{2} qa^2[-2\sin(2\omega t)] \tag{3.42}$$

$$Q_{xy} = -3qa^2 \sin(2\omega t) \tag{3.43}$$

Where we recall that $Q_{xy} = Q_{yx}$, meaning we have found the final two pieces of our quadrupole moment tensor! It turns out they too are time-dependent and therefore radiative. Our assembled matrix appears as follows,

$$Q_{ij} = qa^2 \begin{pmatrix} 1+3\cos(2\omega t) & -3\sin(2\omega t) & 0 \\ -3\sin(2\omega t) & 1-3\cos(2\omega t) & 0 \\ 0 & 0 & -2 \end{pmatrix}. \tag{3.44}$$

3.4 Electric Quadrupole Radiation

For calculations regarding our radiation, it is only necessary to examine the time-dependent entries. Therefore, for our purposes, the matrix simplifies to

$$Q_{ij}(t) = 3qa^2 \begin{pmatrix} \cos(2\omega t) & -\sin(2\omega t) & 0 \\ -\sin(2\omega t) & -\cos(2\omega t) & 0 \\ 0 & 0 & 0 \end{pmatrix}. \tag{3.45}$$

Now, utilizing the fact that the vector potential of a radiating quadrupole is described by the equation

$$\vec{A} = -\frac{\mu_0}{24\pi} ck^2 \frac{e^{ikr}}{r} \vec{Q}(\hat{k}). \tag{3.46}$$

[14] Where, $\vec{Q}(\hat{k})$ is the quadrupole radiation vector which can be represented as

$$\vec{Q}(\hat{k}) = Q_{ij}(t)\hat{k}. \tag{3.47}$$

In an effort to neatly explore the angular dependence of our rotating quadrupole, we will convert $\hat{k}$ from the Cartesian coordinates of our initial system to spherical coordi-

nates.

$$\hat{k} = \begin{pmatrix} x \\ y \\ z \end{pmatrix} = \begin{pmatrix} \sin(\theta)\cos(\phi) \\ \sin(\theta)\sin(\phi) \\ \cos(\theta) \end{pmatrix} \tag{3.48}$$

Carrying out the multiplication to evaluate $\vec{Q}(\hat{k})$, we find

$$\vec{Q}(\hat{k}) = 3qa^2 \begin{pmatrix} \cos(2\omega t) & -\sin(2\omega t) & 0 \\ -\sin(2\omega t) & -\cos(2\omega t) & 0 \\ 0 & 0 & 0 \end{pmatrix} \begin{pmatrix} \sin(\theta)\cos(\phi) \\ \sin(\theta)\sin(\phi) \\ \cos(\theta) \end{pmatrix} \tag{3.49}$$

$$\vec{Q}(\hat{k}) = 3qa^2 \begin{pmatrix} \cos(2\omega t)\sin(\theta)\cos(\phi) - \sin(2\omega t)\sin(\theta)\cos(\phi) \\ -\sin(2\omega t)\sin(\theta)\cos(\phi) - \cos(2\omega t)\sin(\theta)\sin(\phi) \\ 0 \end{pmatrix}. \tag{3.50}$$

Rearranging, and factoring out the common $\sin(\theta)$

$$\vec{Q}(\hat{k}) = 3qa^2 \ \sin(\theta) \begin{pmatrix} \cos(2\omega t)\cos(\phi) - \sin(2\omega t)\cos(\phi) \\ -[\sin(2\omega t)\cos(\phi) + \cos(2\omega t)\sin(\phi)] \\ 0 \end{pmatrix}. \tag{3.51}$$

Now, once again using our friendly neighborhood sum and difference trig identities, the matrix simplifies to

$$\vec{Q}(\hat{k}) = 3qa^2 \ \sin(\theta) \begin{pmatrix} \cos(2\omega t + \phi) \\ -\sin(2\omega t + \phi) \\ 0 \end{pmatrix}. \tag{3.52}$$

Further simplifying the elements inside the vector, we can expand each entry into Euler's Formula, factor that out, and recover the original terms by taking the real part of the expression.

$$\vec{Q}(\hat{k}) = 3qa^2 \ \sin(\theta) \begin{pmatrix} \cos(2\omega t + \phi) + i\sin(2\omega t + \phi) \\ i[\cos(2\omega t + \phi) + i\sin(2\omega t + \phi)] \\ 0 \end{pmatrix} \tag{3.53}$$

$$\vec{Q}(\hat{k}) = 3qa^2 \ \sin(\theta) \begin{pmatrix} e^{i(2\omega t+\phi)} \\ ie^{i(2\omega t+\phi)} \\ 0 \end{pmatrix} \tag{3.54}$$

$$\vec{Q}(\hat{k}) = 3qa^2 \ \sin(\theta) \ e^{i(2\omega t+\phi)} \begin{pmatrix} 1 \\ i \\ 0 \end{pmatrix} \tag{3.55}$$

Separating the exponential sum and explicitly rewriting in terms of our unit vectors as described by the previous vector components,

$$\vec{Q}(\hat{k}) = 3qa^2 \ \sin(\theta) \ e^{i2\omega t} e^{i\phi} (\hat{x} + i\hat{y}). \tag{3.56}$$

Finally, having derived the quadrupole radiation vector, we can continue evaluating the previously expressed equation for vector potential

$$\vec{A}(\vec{r},t) = -\frac{\mu_0}{24\pi} ck^2 \ \frac{e^{ikr}}{r} \vec{Q}(\hat{k}). \tag{3.57}$$

Substituting in Eq. 3.56,

$$\vec{A}(\vec{r},t) = -\frac{\mu_0}{24\pi} ck^2 \ \frac{e^{ikr}}{r} \ 3qa^2 \ \sin(\theta) \ e^{i2\omega t} e^{i\phi} (\hat{x} + i\hat{y}). \tag{3.58}$$

However, spherical polar coordinates prove to be the superior choice of coordinate representation for this angularly dependent vector potential. Therefore, let's rewrite our current set of coordinates in that basis.

$$\hat{x} = \sin(\theta)\cos(\phi)\hat{r} + \cos(\theta)\cos(\phi)\hat{\theta} - \sin(\phi)\hat{\phi} \tag{3.59}$$

$$\hat{y} = \sin(\theta)\sin(\phi)\hat{r} + \cos(\theta)\sin(\phi)\hat{\theta} + \cos(\phi)\hat{\phi} \tag{3.60}$$

In the effort to transform our original $\hat{x} + i\hat{y}$ coordinates, let's break down the complex sum of each $\hat{r}$, $\hat{\theta}$, and $\hat{\phi}$ term independently.

$$\hat{r}: \ \ \sin(\theta)\cos(\phi)\hat{r} + i\sin(\theta)\sin(\phi)\hat{r} \ = \ [cos(\phi) + i\sin(\phi)]\sin(\theta) \ \hat{r} \tag{3.61}$$

$$\hat{\theta}: \ \cos(\theta)\cos(\phi)\hat{\theta} + i\cos(\theta)\sin(\phi)\hat{\theta} \ = \ [\cos(\phi) + i\sin(\phi)]\cos(\theta)\ \hat{\theta} \tag{3.62}$$

$$\hat{\phi}: \ -\sin(\phi)\hat{\phi} + i\cos(\phi)\hat{\phi} \ = \ i[\cos(\phi) + i\sin(\phi)]\ \hat{\phi} \tag{3.63}$$

Now, we can use Euler's identity to factor out a common exponential from each component.

$$(\hat{x} + i\hat{y}) = e^{i\phi}[\sin(\theta)\ \hat{r} + \cos(\theta)\hat{\theta} + i\hat{\phi}] \tag{3.64}$$

Finalizing our transformed spherical coordinate expression for the vector potential

$$\vec{A}(\vec{r},t) = -\frac{\mu_0}{8\pi}ck^2\ \frac{e^{ikr}}{r}\ qa^2\ \sin(\theta)\ e^{i2\omega t}e^{i2\phi}\ [\sin(\theta)\ \hat{r} + \cos(\theta)\hat{\theta} + i\hat{\phi}]. \tag{3.65}$$

With the vector potential out of the way, it is time to tackle the propagating electric and magnetic fields created by our rotating charges. We can express the radiated magnetic field in terms of our vector potential

$$\vec{B}(\vec{r},t) \ = \ i\vec{k} \times \vec{A}(\vec{r},t). \tag{3.66}$$

Where $\vec{k} = k\hat{r}$. Substituting in our expression for $\vec{A}(\vec{r},t)$,

$$\vec{B}(\vec{r},t) \ = \ -i\ \frac{\mu_0}{8\pi}ck^3\ \frac{e^{ikr}}{r}\ qa^2\ \sin(\theta)\ e^{i2\omega t}e^{i2\phi}\ \ \hat{r} \times [\sin(\theta)\ \hat{r} + \cos(\theta)\hat{\theta} + i\hat{\phi}] \tag{3.67}$$

$$\vec{B}(\vec{r},t) \ = \ -i\ \frac{\mu_0}{8\pi}ck^3\ \frac{e^{ikr}}{r}\ qa^2\ \sin(\theta)\ e^{i2\phi}\ \ [\cos(\theta)\hat{\phi} - i\hat{\theta}]\ e^{i2\omega t} \tag{3.68}$$

Now, from the magnetic field, we can derive our radiating electric field.

$$\vec{E}(\vec{r},t) \ = \ -c\hat{k} \times \vec{B}(\vec{r},t). \tag{3.69}$$

$$\vec{E}(\vec{r},t) \ = \ i\ \frac{\mu_0}{8\pi}c^2k^3\ \frac{e^{ikr}}{r}\ qa^2\ \sin(\theta)\ e^{i2\phi}\ \ \hat{r} \times [\cos(\theta)\hat{\phi} - i\hat{\theta}]\ e^{i2\omega t} \tag{3.70}$$

$$\vec{E}(\vec{r},t) \ = \ -i\ \frac{\mu_0}{8\pi}c^2k^3\ \frac{e^{ikr}}{r}\ qa^2\ \sin(\theta)\ e^{i2\phi}\ \ [\cos(\theta)\hat{\theta} + i\hat{\phi}]\ e^{i2\omega t} \tag{3.71}$$

Notably, one of the key takeaways from this model is the frequency of the Electric

and Magnetic field's oscillations. The electromagnetic waves produced from this model have a frequency of 2ω, or in other words, twice the orbital frequency of the binary black holes. Holy Moly! This radiation can directly communicate the orbital frequency of binary pairs of black holes, something we have (to this point) relied entirely on gravitational waves for. Much like with gravitational waves, the in-spiral of two black holes could be monitored via the evolution of this radiation's frequency. The implications of this correlation and example signal characteristics will be further explored in the next chapter.

3.5 Quadrupolar Power Radiated

Finally, in our last act of quadrupolar acrobatics, we will determine the power radiated per unit solid angle for our system of rotating charges. The necessary equation as found in [14] is written

$$\left(\frac{dP}{d\Omega}\right)_{E2} = \frac{\mu_0 c^3 k^6}{1152\pi^2}\left(|Q|^2 - |\hat{r}\cdot\vec{Q}|^2\right). \tag{3.72}$$

Focusing first on the calculation of the quadrupole radiation vector related terms,

$$|Q|^2 = \vec{Q}\cdot\vec{Q}^* \tag{3.73}$$

Where $\vec{Q}^*$ denotes the vector whose entries are the corresponding complex conjugates to the entries of $\vec{Q}$.

$$|Q|^2 \;=\; 9q^2a^4\,\sin^2(\theta)\,[\sin(\theta)\,\hat{r}+\cos(\theta)\hat{\theta}+i\hat{\phi}]\cdot[\sin(\theta)\,\hat{r}+\cos(\theta)\hat{\theta}-i\hat{\phi}] \tag{3.74}$$

$$|Q|^2 \;=\; 9q^2a^4\,\sin^2(\theta)\,[\sin^2(\theta)+\cos^2(\theta)+1] \tag{3.75}$$

$$|Q|^2 \;=\; 9q^2a^4\,\sin^2(\theta)\,[1+1] \tag{3.76}$$

$$|Q|^2 \;=\; 18q^2a^4\,\sin^2(\theta) \tag{3.77}$$

Onto our second term.

$$|\hat{k}\cdot Q|^2 = \left|3qa^2\ \sin(\theta)\ e^{i2\omega t}e^{i2\phi}\ \hat{r}\cdot[\sin(\theta)\ \hat{r}+\cos(\theta)\hat{\theta}+i\hat{\phi}]\right|^2 \tag{3.78}$$

$$|\hat{k}\cdot Q|^2 = \left|3qa^2\ \sin^2(\theta)\ e^{i2\omega t}e^{i2\phi}\right|^2 \tag{3.79}$$

$$|\hat{k}\cdot Q|^2 = 9q^2a^4\ \sin^4(\theta) \tag{3.80}$$

Constructing the full equation with our newly derived components we find

$$\left(\frac{dP}{d\Omega}\right)_{E2} = \frac{\mu_0 c^3 k^6}{1152\pi^2}\left(18q^2a^4\ \sin^2(\theta) - 9q^2a^4\ \sin^4(\theta)\right) \tag{3.81}$$

$$\left(\frac{dP}{d\Omega}\right)_{E2} = \frac{9q^2a^4\mu_0 c^3 k^6}{1152\pi^2}\left(2\ \sin^2(\theta) -\ \sin^4(\theta)\right). \tag{3.82}$$

Simplifying the trigonometric terms,

$$\left(2\ \sin^2(\theta) -\ \sin^4(\theta)\right) = \sin^2(\theta)\left(2-\sin^2(\theta)\right) \tag{3.83}$$

$$= \left(1-\cos^2(\theta)\right)\left(2-1+\cos^2(\theta)\right) \tag{3.84}$$

$$= \left(1+\cos^2(\theta)-\cos^2(\theta)-\cos^4(\theta)\right) \tag{3.85}$$

$$= \left(1-\cos^4(\theta)\right). \tag{3.86}$$

Finally substituting back into our complete equation, we find

$$\left(\frac{dP}{d\Omega}\right)_{E2} = q^2a^4\frac{\mu_0 c^3 k^6}{128\pi^2}\ \left(1-\cos^4(\theta)\right). \tag{3.87}$$

Note that the power radiated per unit solid angle scales exponentially with both charge (in our case charge being absorbed by each black hole), and the orbital radius between both black holes. Additionally, the magnitude is governed by an angular dependence with respect to the plane of our rotating BH's. On the orbital plane, the power radiated is maximized, and as you move off the plane the power radiated falls reaching a minimum of zero perpendicular to the orbital plane. A visualization of this radiation pattern can be seen in Figures 6 and 7.

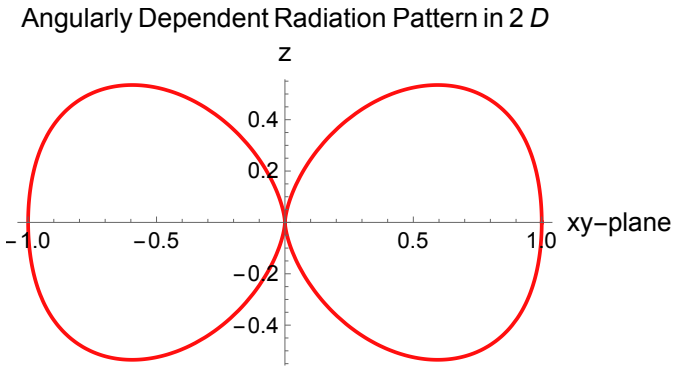

Figure 6: Radiation power diagram expressing the orbital plane of the binary black holes on the horizontal axis.

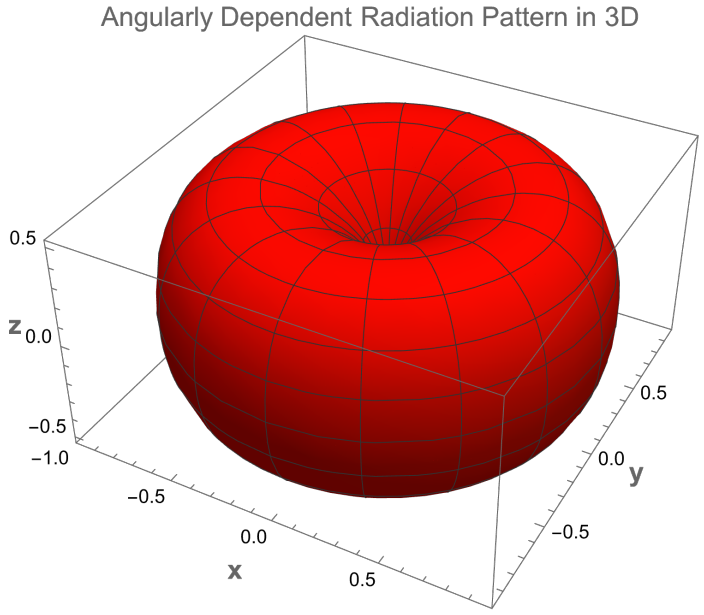

Figure 7: Radiation power diagram expanded into three dimensions, providing an improved spatial intuition of the radiation pattern of the binary black hole system.

In addition to the power radiated per unit angle, we can also calculate the average power radiated by the system across all angles. To do so, we take our expression from Eq. 3.87, and integrate over $d\Omega$.

$$\bar{P} = \int d\Omega \frac{dP}{d\Omega} \tag{3.88}$$

Recalling that $d\Omega = \sin(\theta)\, d\theta d\phi$,

$$\bar{P} = \int \sin(\theta)\, d\theta d\phi q^2 a^4 \frac{\mu_0 c^3 k^6}{128\pi^2} \left(1 - \cos^4(\theta)\right) \tag{3.89}$$

$$\bar{P} = q^2 a^4 \frac{\mu_0 c^3 k^6}{128\pi^2} \int_0^{2\pi} \int_0^{\pi} d\theta d\phi \left(\sin(\theta) - \sin(\theta)\cos^4(\theta)\right) \tag{3.90}$$

$$\bar{P} = q^2 a^4 \frac{\mu_0 c^3 k^6}{128\pi^2}\, 2\pi \left[\int_0^{\pi} d\theta \sin(\theta) - \int_0^{\pi} d\theta\, \sin(\theta)\cos^4(\theta)\right] \tag{3.91}$$

$$\bar{P} = q^2 a^4 \frac{\mu_0 c^3 k^6}{128\pi^2}\, 2\pi \left[-\cos(\theta)|_0^{\pi} + \frac{\cos^5(\theta)}{5}\bigg|_0^{\pi}\right] \tag{3.92}$$

$$\bar{P} = q^2 a^4 \frac{\mu_0 c^3 k^6}{128\pi^2}\, 2\pi \left[2 - \frac{2}{5}\right] \tag{3.93}$$

$$\bar{P} = q^2 a^4 \frac{\mu_0 c^3 k^6}{40\pi} \tag{3.94}$$

Rewriting in terms of ω rather than k for a simpler expression of dependencies in regard to our system.

$$\bar{P} = q^2 a^4 \omega^6 \frac{\mu_0}{40\pi c^3} \tag{3.95}$$

As we can see, the average power radiated is simply an expression which depends on the charge absorbed by each black hole, the radius of the binary orbit, and the frequency of the orbit.

CHAPTER 4

EXPLORING THE UPPER LIMIT OF OUR MODEL

4.1 Summary of Chapter 3 Significant Results

A quick summary of the significant results from the previous calculation-heavy chapter.

1. Our model exhibits a dominant electric quadrupole moment that radiates with frequency 2ω (twice the orbital frequency of our binary black holes). Eqns.3.68 3.71

2. The radiation pattern has a $1-\cos^4(\theta)$ dependence on θ, the elevation angle with respect to the orbital plane. Fig. 6

3. The average power radiated is a function of charge absorbed by each black hole, orbital radius, and orbital frequency of the black hole pair. The expression is written as:

$$\bar{P} = q^2 a^4 \omega^6 \frac{\mu_0}{40\pi c^3}$$

Our goal now is to derive an upper limit for average radiated power, and then employ all that we have learned to construct and investigate sample signals.

4.2 Eddington Accretion Limit

First and foremost, I would like to address the fact that this "upper bound" we will derive is in fact quite... squishy. Accretion disk physics and super-Eddington accretion rates

are still active areas of research, and the scope of this paper is not to break new ground on those fronts. The aim of imposing such a limit is simply to gain some intuition into the conceivable magnitudes of radiative power from the previously derived mechanism.

The Eddington limit is, at its core, a limit on the luminosity of a stellar body considering the outward radiation pressure and the opposing gravitational force. As infalling matter is accelerated towards the massive body (for us a black hole), the particles gain kinetic energy. However, the energized particles interact and their motions change as they dart through this accelerated particle soup. These interactions increase the thermal energy of the infalling particles, and depending on the system, can heat the surrounding matter up to millions of degrees! As a result, the matter radiates thermally and the outgoing photons are scattered off the surrounding particles, introducing the aforementioned radiation pressure. If enough heated material finds itself close to the massive object the radiation pressure overcomes the gravitational influence and surrounding infalling matter is pushed away. Assuming a sufficient supply of surrounding matter, this leads to a natural hydrostatic equilibrium between gravity and radiation pressure. The described balance is (almost) the Eddington limit. The general formula that describes this relationship is written as

$$L = \frac{4\pi GMc}{\kappa}. \tag{4.1}$$

Where L is the luminosity, M is the mass of the massive object, c is the speed of light, and κ is the opacity of the surrounding matter. [16]

Opacity is related to the scattering cross-section for a given cosmic medium. For example, in a simple model, if a collection of ionized hydrogen surrounds a black hole, the associated opacity is a function of the free electron scattering cross-section and the free electron density [17]. It is a measure of how much outgoing radiation energy will be absorbed by the surrounding particle distribution. The true Eddington limit, referred to as the Classical Eddington Limit, is the form of Eq. 4.1 that solely considers free

electron scattering (aka Thompson Scattering) dependent opacity [16]. The Eddington Limit or Eddington Luminosity can be expressed as

$$L_{Edd} = \frac{4\pi cGM}{\kappa_T}. \tag{4.2}$$

When constructing a specialized model with the intent to more accurately approximate the properties of a stellar material, additional scattering mechanisms can be considered when deriving opacity, κ. [18] The Thompson Scattering, however, is a suitable enough approximation for many high-temperature systems [16]. So, in the interest of simplicity we will only consider Thompson free electron scattering for our squishy upper limit.

In addition to our current expression for luminosity, we need to expand the formulation to include the accretion, or rate of mass absorption, dependent luminosity associated specifically with black holes. The same thermal radiation pressure is present for compact massive objects like black holes, however, the increased gravitational potential close to the object allows for higher temperatures of accelerating matter and in turn, tremendously high luminosities. [16] The equation describing luminosity for an accreting body is

$$L_{accretion} = \varepsilon \dot{M} c^2 \tag{4.3}$$

Where again, $L_accretion$ represents luminosity, $\dot{M}$ is the accretion rate of matter, and ε corresponds to the radiative efficiency of the accretion process. Accretion efficency is described as the component of the matter's rest mass energy which is radiated away, and is most often set to $\varepsilon = 0.1$ for systems considering a black hole accreting matter through a disk [16].

We now have two expressions for luminosity, the limiting Eddington Luminosity and the luminosity associated with an accretion process. Let us equate the two to derive

an upper limit on the accretion rate of a black hole.

$$\varepsilon \dot{M} c^2 = \frac{4\pi c G M}{\kappa_T} \tag{4.4}$$

$$\dot{M} = \frac{4\pi G M}{\varepsilon \kappa_T c} \tag{4.5}$$

Utilizing the fact that $G = \frac{4\pi^2}{M_\odot} \frac{AU^3}{year^2}$, we can rearrange our equation.

$$\dot{M} = \frac{16\pi^3}{\varepsilon \kappa_T c} \frac{AU^3}{year^2} \frac{M}{M_\odot} \tag{4.6}$$

Assuming our accretion disk is composed of fully ionized hydrogen, the Thompson scattering dependent opacity takes on the value $\kappa = 0.4 \frac{cm^2}{g}$. Additionally, using the previously quoted $\varepsilon = 0.1$ efficiency value, and a few unit conversions, we arrive at the equation

$$\dot{M} = \frac{16\pi^3 \ [149,597,870,700\ m]^2}{[0.1][0.4 \frac{cm^2}{g} \times (\frac{1\ m}{100\ cm})^2][3 \times 10^8 \ \frac{m}{s}][1\ year \times \frac{3.154 \times 10^7}{1\ year}]^2} \frac{M}{M_\odot}. \tag{4.7}$$

Which evaluates to

$$\dot{M} = 1.4 \ \times 10^{18} \ \frac{M}{M_\odot} \frac{g}{s}. \tag{4.8}$$

Outstanding! Now we have an expression which tells us the rate at which our black holes can absorb the surrounding plasma. It is worth noting, however, the sweeping nature of the binary black holes likely implies that a component of the swallowed plasma falls directly into the black hole rather than a decaying orbital motion. This direct infall could generate Super-Eddington accretion rates, however that would increase the charge consumed transitively increasing the radiated power of our quadrupolar mechanism under investigation. Therefore, considering super-eddington effects only aids in the intensity of our radiation, I will use this conservatively derived upper accretion limit for our purposes.

4.3 Implications of the Derived Accretion Rate

Given the previously derived accretion limit in Eq. 4.8, we can evaluate the mass of plasma absorbed by each of our binary black holes over one orbital cycle. The period of each black hole's orbital motion is described by $T = \frac{1}{\omega}$, where once again ω is the orbital frequency of our black holes. Therefore, if our black holes are accreting at the Eddington Limit, the swallowed matter in a given orbital cycle is given by the equation

$$M_{cycle} = 1.4 \times 10^{18} \frac{M}{M_{\odot}} \frac{g}{s} \times \frac{1}{\omega}. \tag{4.9}$$

Allow me to motivate the coming discussion on the basis of expressing q, the charge absorbed by each black hole in our model, in terms of the limiting accretion rate above. If we succeed, we will have an upper bound for q that allows us to further explore the properties of our proposed radiation.

Extrapolating this M_{cycle} result into the average instantaneous charge absorbed by each black hole at any given point in their orbits requires an investigation of the associated volumes. If each black hole acts as an absorbing sphere whose radius is that of the BH's innermost stable circular orbit, then we also know that over the time of each cycle the binary orbit of that black hole will have carved out a toroidal volume. The volume of our (ideally spherical) plasma hole is given by

$$V_{Hole} = \frac{4}{3} \pi r_{ISCO}^3, \tag{4.10}$$

and the volume of a torus is given by

$$V_{Torus} = (2\pi a)(\pi r_{ISCO}^2). \tag{4.11}$$

Where the first component in our expression of the toroidal volume corresponds to the circumference traced by our BH's orbital motion with radius a, and the second component describes the area of the circle along that circumference determined by our BH's ISCO.

Having derived the mass of plasma absorbed by each black hole over one orbital orbital cycle (Eqn.4.9) and now having an expression for the volume traced over one cycle (Eqn. 4.11), we can describe the plasma absorbed per unit volume as

$$\frac{M_{cycle}}{V_{Torus}} = \frac{M_{Cycle}}{2\pi^2\, a\, r_{ISCO}^2} \tag{4.12}$$

Note that this faux plasma density is simply a calculational tool allowing us to express a time-dependent process such as accretion in terms of the instantaneous charge absorbed at any given time. Moreover, this mathematical plasma density is NOT the density of plasma inside a black hole, it is simply a geometric bookkeeping trick. Moving on.

The ratio of mass of absorbed per unit volume is a simple proportion that holds true for any corresponding mass/volume pair in this system. Therefore, we will construct the proportion

$$\frac{M_{Hole}}{V_{Hole}} = \frac{M_{cycle}}{V_{Torus}}. \tag{4.13}$$

Substituting in our equation for V_{Hole} and V_{Torus} we find

$$\frac{M_{Hole}}{\frac{4}{3}\pi\, r_{ISCO}^3} = \frac{M_{cycle}}{2\pi^2\, a\, r_{ISCO}^2} \tag{4.14}$$

$$M_{Hole} = \frac{2}{3}\,\frac{r_{ISCO}}{\pi a}\, M_{cycle} \tag{4.15}$$

This expression tells us that the average mass of plasma contained in the superimposed orbiting plasma spheres earlier addressed in this theory (which we have since simplified to rotating points of charge in our mathematical model) can be represented as a fraction of the mass absorbed each orbital cycle scaled by the ratio of ISCO radius to the binary BH's orbital radius.

Depending on the characteristics of a black hole, the size of its innermost stable circular orbit varies. For example, the ISCO of a non-rotating black hole with no charge (Schwarzschild Black Hole) is described by the equation

$$r_{ISCO} = 6km\,\frac{M}{M_\odot} \tag{4.16}$$

[8]. As different properties of the black hole's charge and spin are considered, this relation ranges anywhere from $1-9km\,\frac{M}{M_\odot}$. We will continue with the relation associated with a Schwarzschild Black Hole, but this is a trivial swap if one wishes to explore a black hole of particular type.

Expanding our entire expression for the mass of plasma enclosed by our spherical volume, we find

$$M_{Hole} \;=\; \frac{2}{3}\left[\frac{6\;km\;\frac{M}{M_\odot}}{\pi a}\right]\left[1.4\;\times 10^{18}\;\frac{M}{M_\odot}\frac{g}{s}\times\frac{1}{\omega}\right] \tag{4.17}$$

$$M_{Hole} \;=\; \frac{5.6\;\times 10^{18}\;\frac{km\;g}{s}}{\pi a\omega}\;\left[\frac{M}{M_\odot}\right]^2 \tag{4.18}$$

Which at long last will allow us to extract the charge enclosed in our plasma spheres. One assumption we will make here is that the plasma being consumed by the black hole is mostly comprised of protons. This is a valid assumption for several reasons. First, from the notion of radiation pressure regulating the influx of accreted matter, the radiation pressure can be predicted to have a more significant impact on the surrounding electrons seeing as though their masses are significantly smaller. This allows protons to persist through the high pressures approaching the black hole where electrons are more likely to be blown away. Additionally, for the sake of an upper limit, it is worth exploring the case when the black hole is accreting uniformly charged matter. That being said, let us break down the derived mass into individual protons and asses the total charge from proton count.

$$q_{plasma} \;=\; \frac{M_{Hole}}{m_p}\;q_p \tag{4.19}$$

Where the mass in our plasma sphere is divided by the mass of a proton to yield the number of protons present. From there, the proton number is then multiplied by the charge of a single proton to find the total charge. Expanding the relation we see

$$q_{plasma} \;=\; 5.6\;\times 10^{18}\;\frac{km\;g}{s}\;\frac{q_p}{\pi a\omega\;m_p}\;\left[\frac{M}{M_\odot}\right]^2. \tag{4.20}$$

An expression for the plasma ”missing” from the accretion disk at any given time due to a black hole consuming matter at the Eddington limit. With this result, we can construct a complete sample signal from the radiative quadrupole moment model derived in Chapter 3.

CHAPTER 5

CHARACTERISTIC PROPERTIES OF A SAMPLE RADIATION SIGNAL

5.1 Calibration of our Binary System Inputs

For the construction of our sample signal, we will be considering a binary system of black holes with mass $M_1 = M_2 = 30M_\odot$. This system is similar to the original binary black hole merger discovered by LIGO in 2015. Their binary system consisted of a $36M_\odot$ black hole and its accompanying $29M_\odot$ black hole companion [19]. The characteristic frequency "chirp" associated with the accelerating orbital frequency during binary black hole mergers can be visualized in spectrogram of the 2015 LIGO event found in Fig. 8.

In an attempt to capture this frequency evolution in our sample signal, we will fit a model frequency curve to the pattern seen in Fig. 8 in order to create a realistic evolution of our own binary system's orbital frequency. Recalling that gravitational radiation is quadrupolar, much like the radiative mechanism we are exploring now, the gravitational radiation frequencies from Fig. 8 represent twice the orbital frequency. The LIGO report claims that the orbital frequency should rise from 17.5 Hz to 75 Hz in 0.2 seconds, which is reflected in the modeled frequency chirp shown in Fig. 9

In addition, we must consider the shrinking orbital radius of the system. The orbit shrinks due to the gravitational waves radiating energy away from the system. As the inspiral continues, the gravitational waves grow more pronounced radiating away more energy, leading to an aggressive and swift merger as we can infer from the frequency

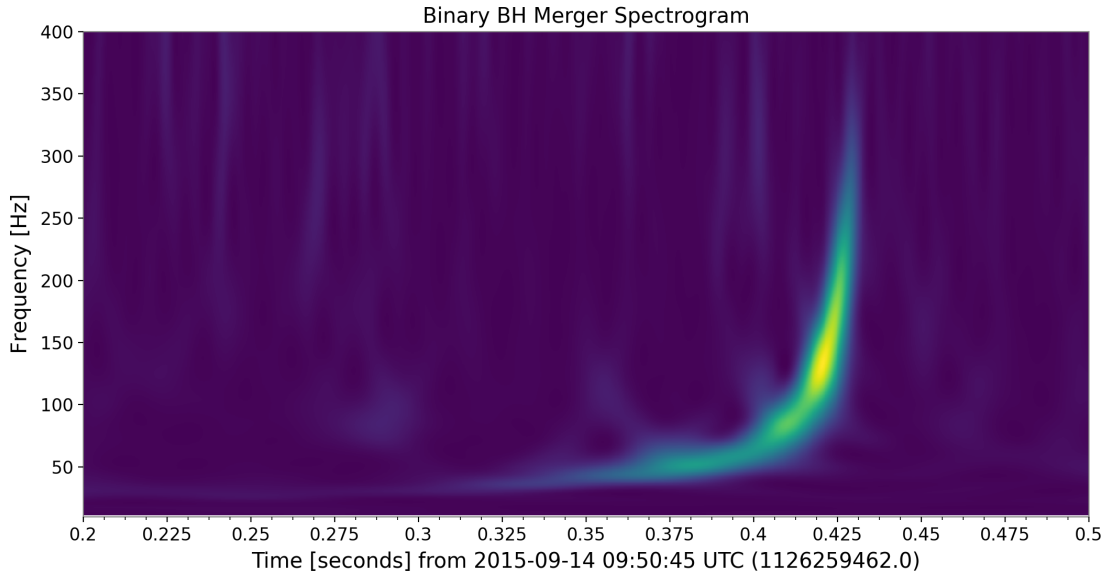

Figure 8: Plot depicting the frequency evolution of two merging black holes. Graphic created using the Gravitational Wave Open Science Center's data analysis tool based on the first recorded LIGO event [19].

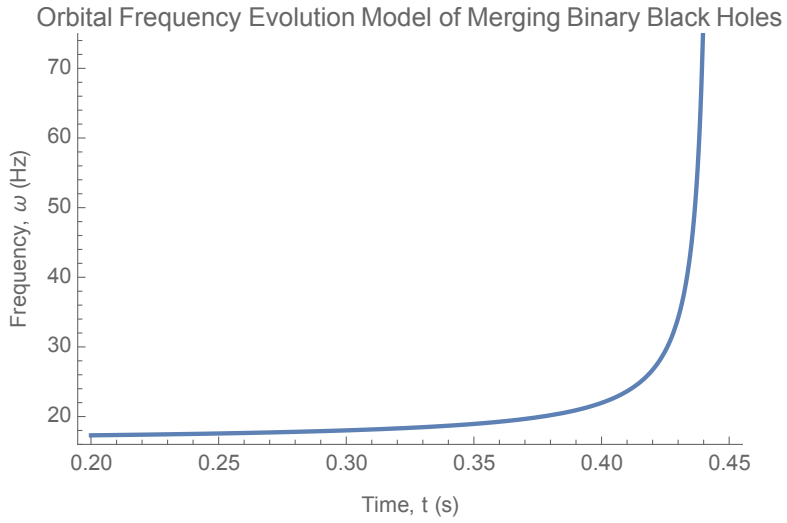

Figure 9: Binary black hole orbital frequency model which will be used to evolve the derived parameters of our radiation from Chapter 3. The equation used to fit this model: $\left[\omega = -\frac{1}{4(t-0.444)} + 16.28\right]$

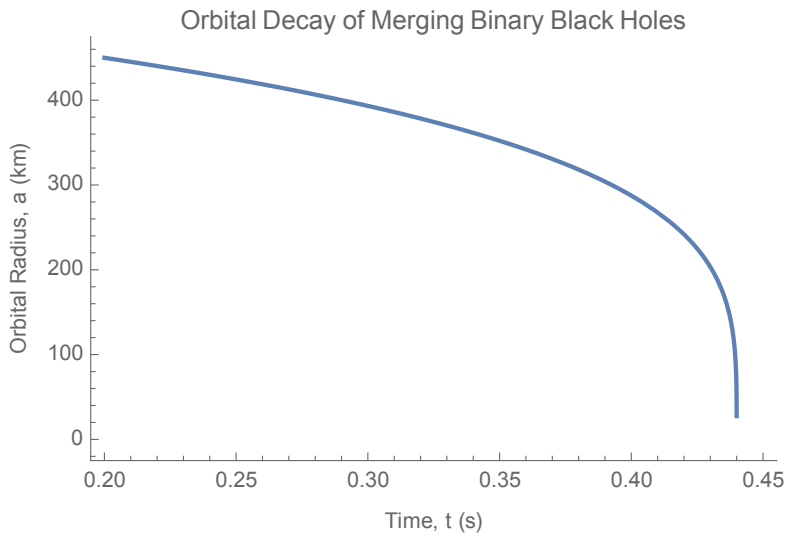

Figure 10: Binary black hole orbital radius model which will be used to evolve the derived parameters of our radiation from Chapter 3.

chirp spectogram. The shrinking orbital radius is approximated by the equation

$$a = a_0 \left(1 - \frac{t - t_0}{\tau}\right) \tag{5.1}$$

Where a_0 is the starting radius, t_0 is the starting time, and τ is the characteristic time scale of the merger [20]. For the sample case currently being considered, we will set $t_0 = 0.2s$, $\tau = 0.24s$, and the report from ligo claims an initial orbital radius of roughly 5 R_s (R_s refers to the Schwarzschild Radius) [19]. As we are considering two Schwarzschild black holes with Masses $M_1 = M_2 = 30M_\odot$, the Schwarzschild Radius $R_s = 3\frac{km}{M_\odot}$ simply evaluates to $R_s = 90km$. Substituting into our expression, we find

$$a = 450km \left(1 - \frac{t - 0.2s}{0.24s}\right) \tag{5.2}$$

Which produces a decaying orbital radius of the form seen in Fig. 10.

5.2 Sample Signal

With the foundations of our sample signal in place, we can evaluate the characteristic charge evolution in our rotating point charge model, along with the frequency and average power radiated of the resulting radiation.

The charge evolution for both point charges in the model is governed by the equation

$$q_{plasma} = 5.6 \times 10^{18} \frac{km\ g}{s} \frac{q_p}{\pi a \omega\ m_p} \left[\frac{M}{M_\odot}\right]^2. \tag{5.3}$$

When evaluated for the current system in consideration we find

$$q_{plasma} = \frac{1.539 \times 10^{26}}{a(t)\ \omega(t)} \frac{km\ C}{s}. \tag{5.4}$$

Which exhibits the inspiral evolution characteristics displayed in Fig. 11. Next, the

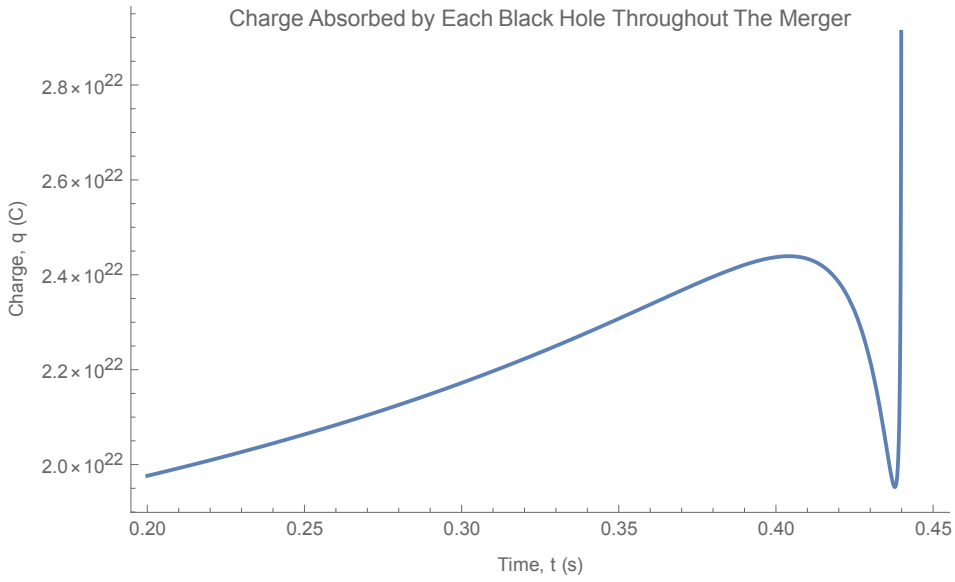

Figure 11: Charged absorbed by each binary black hole throughout the inspiral and merger process. The spike at the end of the plot is an artifact of the orbital radius shrinking to zero.

frequency is a simple case. The radiation's frequency is exactly double the orbital frequency of the black holes. Therefore, our frequency evolution can be observed in Fig. 12 Finally, the average power radiated, a function of the freshly expressed charge, radius,

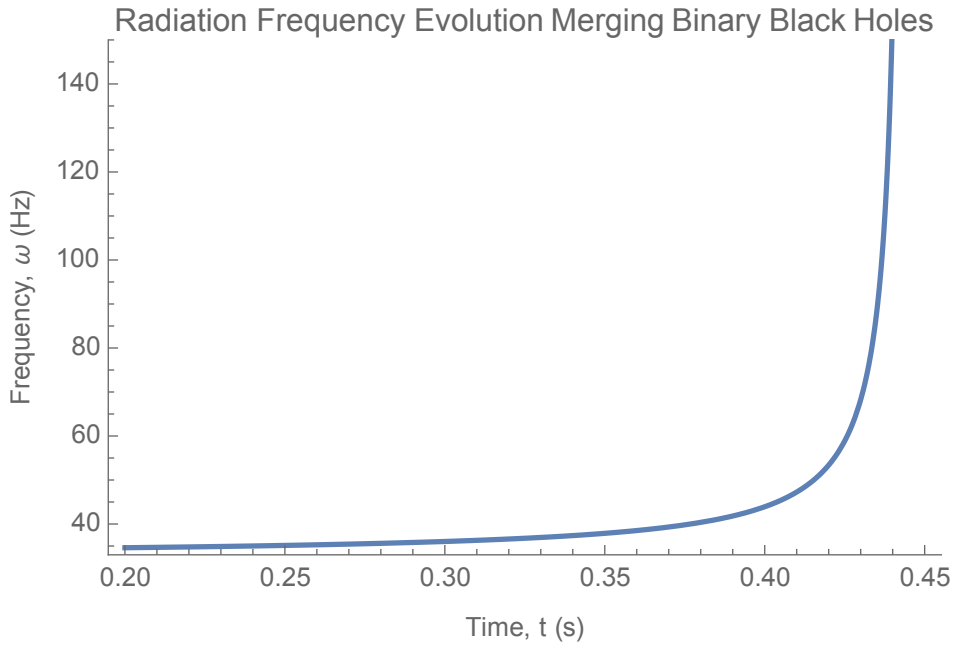

Figure 12: Radiation frequency throughout the inspiral. These frequencies are exactly twice the orbital frequency.

and frequency, is described by the equation

$$\bar{P}(t) = \; q(t)^2 a(t)^4 \omega(t)^6 \frac{\mu_0}{40\pi c^3}. \tag{5.5}$$

Rewriting with values,

$$\bar{P}(t) = 3.7037 \times 10^{-34} \; q(t)^2 a(t)^4 \omega(t)^6 \; \frac{kg\; s^3}{m^2\; C^2} \tag{5.6}$$

The inspiral evolution of our quadrupolar radiated power, dependent on each of our previously derived evolutions, is represented in Fig. 13

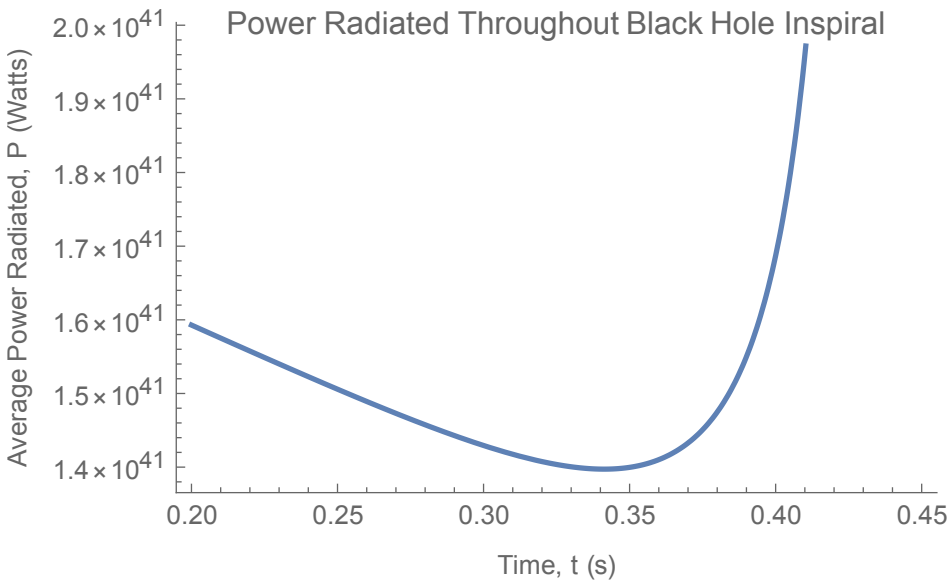

Figure 13: Plot showing the average power radiated of the proposed quadrupolar radiation as it evolves throughout the black hole merger .

CHAPTER 6

CONCLUSION AND OUTLOOK

6.1 Discussion of Results

Over the course of this theoretical investigation, we were able to derive the presence of an electric quadrupolar radiative mechanism in active binary black hole systems whose frequency is directly coupled to the orbital frequency of its host black holes. Additionally, simulating our sample signal, we saw substantial charge absorbed and power radiated values. These calculated upper limiting values, granted, should be viewed with reservations as they are likely in the non-linear regime of electric field strength. It should be noted, the considered case included both of our black holes accreting matter at the Eddington limit, therefore maximizing the possible charge considered in our system. In reality however, accretion disk densities and therefore available plasma around black holes span a dramatic range, some black hole systems are maximally fed to the Eddington Limit while others are entirely inactive. This range indicates that for many sub-Eddington limit accreting black holes our initial linear super position model is applicable and therefore radiation of the form presented in this investigation will occur. The characteristic evolution of our derived quantities throughout the inspiral of the black hole binary also unearthed interesting dependencies between our radiation's properties and the time evolution of frequency and orbital radius during a merger. Additionally, the consistently high power radiated even before the final merger of the black holes suggests a potential area of pre-merger orbital study not previously possible with LIGO due to the irrecoverably low signal strength of pre-merger gravitational waves.

While neither the model nor the assumptions with in it are perfect representations of our true astrophysical system, it is clear that the discussed form of radiation can manifest in active binary black hole systems and furthermore it would radiate at a significant power.

6.2 Future work

In regard to the improvement of our model, several avenues of continued work immediately make themselves apparent to me. Firstly, expanding this formulation to account for differing mass black hole systems, implying variable absorbed charge corotating in non circular orbits, would widen the population of applicable systems dramatically. Additionally, given the incredible charges present in the calculation of our sample signal, surely the next natural step is to re-derive this mechanism accounting for the extreme electric fields present and therefore the emerging non-linearities of the system. Lastly, the expansion of our simplified rotating point charge system to true three dimensional voids representing the carved plasma holes in our accretion disk would more realistically represent the missing charge's effect on the surrounding electric field. While these adjustments do add complexity to the pleasantly simple model presented here, the ability to evaluate more general systems dramatically increase the utility of the model in step.

Notwithstanding these pending improvements, interesting research can already be imagined. An obvious extension of this theoretical formulation into the realm of experimental physics lies within the observability of the proposed radiation. The characteristic frequencies of the radiation emitted by merging black holes would be confined to extremely low frequency (ELF) radio wave range between 3 - 300 Hz. This range of frequencies is associated with wavelengths on the order of 100,000 - 1000 km. As a

first step into the hopeful existential confirmation and future study of the proposed radiation, it is necessary to develop adequate infrastructure to observe some portion of the quoted wavelengths. Once said infrastructure is complete, the detection can be used to compare and supplement LIGO's gravitational wave merger events. More uniquely, the radiation also has potential to expand upon LIGO's current population of observable systems. As mentioned in the discussion above, the system should radiate with significant power long before the merger of the black holes. Such a phenomena implies that unlike the quantum limited strain sensitivity of LIGO which prevents the resolution of any gravitational waves prior to the merger, our radiation would illuminate the orbits of binary black holes long before any such cataclysm.

Further work will be conducted in the continued investigation of our proposed radiation, and any major developments will be communicated in subsequent papers. Thank you for your attention.

Acknowledgment

This research and thesis were made possible by both the generous academic and personal support offered to me on a daily basis by my professors, friends, and family.

My work was founded upon the description of a physical system laid out by my external research advisor Professor Bruno Coppi. He was also kind enough to let me choose my research project and transform it into my own creation. Thank you for allowing me to explore this wonderful subject!

My UMass Boston Professors continue to push me past the boundaries of my current knowledge. The encouraging, engaging, and collaborative environment they create truly lends itself to an unrivaled educational experience. Specifically, I would like to thank Professors Steve Arnason, Chandra Yelleswarapu, John Celli, and Chris Fuchs for hosting a genuinely enlightening suite of graduate courses throughout my master's.

Additionally, Professor Arnason deserves to be thanked again. His class was not only fundamental to the conceptual development of my thesis, but the extra time he gave me after class or during office hours to express my ideas and discuss the formulation laid out in front of you in this document was truly special.

I would like to show my gratitude to my fellow classmates Max and Chris. They might struggle with their homework but they are great friends and support me always.

Finally, I of course must thank all of my loving and supportive family members. My incredible girlfriend who kept me sane throughout the embarrassing number of sleepless nights during this thesis. My parents who have always been there to support me, whether it was baseball, the science fair, or singing Billionaire at the foot of their bed, they were there for me and that has never changed. I don't know where I would be without you.

Nick.

REFERENCE LIST

[1] K. Schwarzschild. “On the gravitational field of a mass point according to Einstein’s theory”. In: *arXiv e-prints*, physics/9905030 (May 1999), physics/9905030. arXiv: physics/9905030 [physics.hist-ph].

[2] J. Kristian et al. “On the Optical Identification of Cygnus X-1”. In: 168 (Sept. 1971), p. L91. DOI: 10.1086/180790.

[3] H. L. Shipman. “The Implausible History of Triple Star Models for Cygnus X-1: Evidence for a Black Hole”. In: 16 (Feb. 1975), p. 9.

[4] S. W. Hawking. “Particle Creation by Black Holes”. In: *Commun. Math. Phys.* 43 (1975). Ed. by G. W. Gibbons and S. W. Hawking. [Erratum: Commun.Math.Phys. 46, 206 (1976)], pp. 199–220. DOI: 10.1007/BF02345020.

[5] S W Hawking. “Black hole explosions?” en. In: *Nature* 248.5443 (Mar. 1974), pp. 30–31.

[6] Event Horizon Telescope Collaboration. *Event Horizon Telescope: Science*. 2023. URL: https://eventhorizontelescope.org/science.

[7] Event Horizon Telescope Collaboration. *Press Release (April 10, 2019): Astronomers Capture First Image of a Black Hole*. 2019. URL: https://eventhorizontelescope.org/press-release-april-10-2019-astronomers-capture-first-image-black-hole.

[8] Ming Zhang and Wen-Biao Liu. “Innermost stable circular orbits of charged spinning test particles”. In: *Physics Letters B* 789 (2019), pp. 393–398. ISSN: 0370-2693. DOI: https://doi.org/10.1016/j.physletb.2018.12.051. URL: https://www.sciencedirect.com/science/article/pii/S0370269318309869.

[9] J. E. Pringle and M. J. Rees. “Accretion Disc Models for Compact X-Ray Sources”. In: 21 (Oct. 1972), p. 1.

[10] D. Mudd et al. “Quasar Accretion Disk Sizes from Continuum Reverberation Mapping from the Dark Energy Survey”. In: 862.2, 123 (Aug. 2018), p. 123. DOI: 10.3847/1538-4357/aac9bb. arXiv: 1711.11588 [astro-ph.GA].

[11] B. Coppi. “Formation and Ejection of Helical Plasma Structures from Gravitational Wave Emitters”. In: *Fundamental Plasma Physics* 4 (2023), p. 100007. ISSN: 2772-8285. DOI: https://doi.org/10.1016/j.fpp.2022.100007. URL: https://www.sciencedirect.com/science/article/pii/S2772828522000073.

[12] Mark Buchanan. “Past the Schwinger limit”. In: *Nature Physics* 2.11 (Nov. 2006), pp. 721–721. ISSN: 1745-2481. DOI: 10.1038/nphys448. URL: http://dx.doi.org/10.1038/nphys448.

[13] Adeogun Christopher O. “The Stability and Behaviour of the Superposition of Non-Linear Waves in Space”. In: *International Journal of Physics Research and Applications* 6.2 (Dec. 2023), pp. 216–221. ISSN: 2766-2748. DOI: 10.29328/journal.ijpra.1001075. URL: http://dx.doi.org/10.29328/journal.ijpra.1001075.

[14] Stephen Arnason. *Class Notes*. Physics 612, Classical Electromagnetism.

[15] E. Alecian. *An Introduction to Accretion Disks*. https://sites.astro.caltech.edu/~lah/review/stardiskphenom_alecian.pdf. [Accessed 13-04-2024].

[16] *The Eddington Limit*. https://jila.colorado.edu/~pja/astr3730/lecture18.pdf. ASTR 3730. 2003.

[17] Rich Townsend. *Introduction to Stellar Astrophysics*. https://www.bartol.udel.edu/~owocki/phys633/14-opacity.pdf. 2006.

[18] D. Heinzeller and W. J. Duschl. "On the Eddington limit in accretion discs". In: *Monthly Notices of the Royal Astronomical Society* 374.3 (Dec. 2006), pp. 1146–1154. ISSN: 0035-8711. DOI: 10.1111/j.1365-2966.2006.11233.x. eprint: https://academic.oup.com/mnras/article-pdf/374/3/1146/3548253/mnras0374-1146.pdf. URL: https://doi.org/10.1111/j.1365-2966.2006.11233.x.

[19] B. P. Abbott et al. "Observation of Gravitational Waves from a Binary Black Hole Merger". In: *Phys. Rev. Lett.* 116 (6 Feb. 2016), p. 061102. DOI: 10.1103/PhysRevLett.116.061102. URL: https://link.aps.org/doi/10.1103/PhysRevLett.116.061102.

[20] Brian D. Farris et al. "Binary black hole accretion during inspiral and merger". In: *Monthly Notices of the Royal Astronomical Society: Letters* 447.1 (Dec. 2014), pp. L80–L84. ISSN: 1745-3925. DOI: 10.1093/mnrasl/slu184. eprint: https://academic.oup.com/mnrasl/article-pdf/447/1/L80/54652970/mnrasl_447_1_l80.pdf. URL: https://doi.org/10.1093/mnrasl/slu184.